Journal of Power Sources 240 (2013) 551–557

Contents lists available at SciVerse ScienceDirect

Journal of Power Sources

journal homepage: www.elsevier.com/locate/jpowsour

Methylated silicon: A longer cycle-life material for Li-ion batteries

Larbi Touahir [a], Abdelhak Cheriet [a,b], Daniel Alves Dalla Corte [a], Jean-Noël Chazalviel [a], Catherine Henry de Villeneuve [a], François Ozanam [a], Ionel Solomon [a], Aissa Keffous [b], Noureddine Gabouze [b], Michel Rosso [a,*]

[a] Physique de la Matière Condensée, CNRS, Ecole Polytechnique, 91128 Palaiseau, France
[b] Centre de Recherche en Technologie des Semi-conducteurs pour l'Énergétique-CRTSE, 02 bd. Frantz Fanon, B.P. 140, Alger 7 Merveilles, Alger, Algeria

HIGHLIGHTS

- Thin layers of amorphous methylated Si were prepared by PECVD.
- We studied this material as a negative electrode material for Li-ion batteries.
- Amorphous methylated Si shows enhanced cyclability compared to pure Si.
- The improvement is attributed to mechanical softening of amorphous Si.

ARTICLE INFO

Article history:
Received 5 December 2012
Received in revised form
18 April 2013
Accepted 21 April 2013
Available online 27 April 2013

Keywords:
Methylated amorphous silicon
Thin-layer
Cyclability
Li-ion batteries

ABSTRACT

Using Plasma Enhanced Chemical Vapor Deposition, one can prepare methylated amorphous silicon thin-layer anodes for Li-ion batteries exhibiting good cyclability. The properties of that material are investigated here in view of this target application. In comparison with pure amorphous silicon prepared in the same conditions, the improvement is twofold: longer lifetime, and capability of working with thicker electrodes. For example, capacity retention after 100 cycles of 150 nm thick layers with 10% carbon content is almost 70% larger than that of pure a-Si layers. The observed improvement is attributed to mechanical softening of amorphous Si by incorporation of CH_3 groups.

1. Introduction

Silicon is considered as a promising anode material for Li-ion batteries because of its unique capability to insert large quantities of lithium: its capacity (about 4000 mA h g^{-1}) is more than ten times as high as that of graphite, which is used in commercial batteries. However, its use is severely limited, due to the important swelling of the material in the loaded state (300%) [1]. Various solutions to this problem were proposed: they require the use of silicon in nanometric form: several reviews summarize the recent literature on this subject [2–4].

Although they are not of practical interest for applications requiring large amounts of energy, thin layers of amorphous silicon are currently studied (see for example Ref. [2]), in particular because they offer a very convenient geometry for many experimental studies. Magnetron sputtering, evaporation, Chemical Vapor Deposition (CVD) were used to produce these layers.

Various treatments of the layers were shown to improve their cyclability [2,5–7]. However, in most cases, the cyclability is strongly reduced upon increasing the layer thickness [8]. Obviously, an improvement of the starting material properties is of great interest. Our aim here is to propose such a new starting material, with a capacity similar to that of silicon and enhanced cyclability.

Amorphous hydrogenated silicon (a-Si:H) is a particular variety of amorphous silicon: it was extensively studied because of its good semiconducting properties, due to its high hydrogen content. Part of these hydrogen atoms are linked to Si atoms, saturating most of the dangling bonds which are present in the non-hydrogenated amorphous material. This lowers the density of electronic states in the forbidden band gap, hence good semiconducting properties are obtained [9]. This semiconductor may be doped either n- or p-type.

* Corresponding author. Tel.: +33 169334667.
E-mail address: michel.rosso@polytechnique.fr (M. Rosso).

0378-7753/$ – see front matter © 2013 Elsevier B.V. All rights reserved.
http://dx.doi.org/10.1016/j.jpowsour.2013.04.089

a-Si:H was also considered as an anode material for Li-ion batteries: for instance, Kulova et al. [10] studied lithium insertion into amorphous hydrogenated silicon prepared by rf glow discharge in silane. They confirmed the cyclability decrease of the layers with increasing their thickness.

The use of heterogeneous mixtures of carbon and silicon (powders of silicon grains surrounded by carbon, etc…) allows for improving the cycling properties of silicon [11]. Such heterogeneous mixtures have focused attention because the stoichiometric alloy SiC (silicon carbide) does not insert lithium. Indeed SiC is known for its electrochemical inactivity and is currently used as an inactive phase in a variety of anode composites (see for example Ref. [12]). However, even in such mixtures, volume changes due to insertion/de-insertion of lithium remain an important issue.

In this paper we disregard these composite materials and consider a particular form of Si–C alloy as an anode material for Li-ion batteries. This alloy is a homogeneous amorphous silicon/carbon based material where the C atoms are inserted into amorphous silicon as methyl groups CH_3. This silicon-rich material can be expected to retain a high lithium-insertion capability. Like silicon–silicon carbide composites it may be expected to exhibit a behavior distinct from that of pure silicon, while avoiding disadvantages associated with heterogeneous mixtures. The purpose of the present work was therefore to investigate the performance of methylated amorphous silicon as a negative electrode material for lithium-ion batteries.

2. Methylated silicon

Thin films of amorphous Si–C alloys can be prepared by simultaneous decomposition of silane and methane obtained by Plasma Enhanced Chemical Vapor Deposition (PECVD). Using this technique, one can obtain a variety of amorphous silicon–carbon alloys [13].

In the present paper, thin films of the amorphous material are obtained in the "low power regime" (plasma power $P < 0.3$ W cm^{-2}) [13,14], where only SiH_4 molecules are decomposed (not CH_4 molecules): carbon incorporation into the amorphous Si layer is then produced by the reaction between methane molecules and active species (radicals) resulting from the decomposition of SiH_4. In this low-power regime the carbon content can only be obtained in a restricted range $x < 0.4$. Carbon atoms are then only or mostly inserted as methyl groups $-CH_3$ [13,15]. The material may thus be described as methylated amorphous silicon, with composition a-$Si_{1-x}(CH_3)_x$:H.

These methyl groups can only be linked to one silicon atom, thus creating dead ends in the silicon network. They were shown to be surrounded by spherical nanovoids [16]. The presence of a majority of silicon atoms should confer a high lithium intercalation capacity to the material. The fact that the carbon content may be continuously tuned between 0 and 0.4 is another advantage, enabling to choose the optimum content for the target application.

For compounds with a proportion of carbon higher than 0.2, not all of the carbon atoms are in CH_3 configuration: part of the carbon atoms is in CH_2 configuration. This is also the case for the material deposited with a high-power plasma ($P > 0.3$ W cm^{-2}): the value of the carbon proportion x may then be obtained in the whole range $0 < x < 1$ [13,14].

The relative proportion of CH_2 and CH_3 configurations was estimated in Ref. [13] from comparison between hydrogen and carbon contents in the material. In the present study, they are directly monitored by infrared spectroscopy measurements (see Section 4).

3. Experimental conditions

Different layers of pure a-Si:H and a-$Si_{1-x}(CH_3)_x$:H were prepared by PECVD in the low-power regime.

For electrochemical measurements, layers with different thicknesses were deposited on stainless steel substrates. Before deposition the substrates were first washed with a concentrated detergent, then rinsed with milli-Q water, and dried with a nitrogen flow. Then they were placed in the PECVD chamber, where they were submitted to a hydrogen plasma (pressure 200 mTorr, power density 100 mW cm^{-2}) for 5–10 min. This pre-treatment enabled good adhesion of the layer. Carbon content in the film was controlled through the gas-phase composition, i.e., [CH_4] partial pressure in the [CH_4][SiH_4] mixture [13]: the investigated carbon contents were $x = 0$, $x = 0.1$, $x = 0.15$, $x = 0.2$, $x = 0.25$ and $x = 0.33$. Thicknesses ranged from 30 to 150 nm for $x = 0$ and from 50 to 600 nm for $x = 0.1$ to 0.2. For $x = 0.25$ and $x = 0.33$, only a restricted series of samples was studied (see below), with thicknesses 45 nm and 30 nm respectively. During film deposition, the substrate temperature was maintained at 250 °C. No intentional doping was performed (i.e., no gas such as B_2H_6 or PH_3 was added to the SiH_4/CH_4 mixture).

Two-electrode half-cells were assembled in order to evaluate the electrochemical properties. The a-$Si_{1-x}(CH_3)_x$:H thin films were used as the working electrode. Li-metal sheet (99.9% purity, Aldrich) was used as the counter electrode. The electrolyte was 1 M $LiClO_4$ (battery grade, 99.99% purity, Aldrich) in propylene carbonate (99.7% purity, Sigma–Aldrich). The cells were cycled galvanostatically. Lithiation of the a-$Si_{1-x}(CH_3)_x$:H electrode was carried out from the initial open-circuit voltage down to 0.025 V, then cycling was performed between 0.025 V and 2 V vs. Li/Li^+. Cells were tested at various charge/discharge current densities in the C/0.5–C/10 range (full charge or discharge in 0.5–10 h, corresponding to current densities from 2 to 50 μA cm^{-2}, depending on carbon content and film thickness). A multi-channel potentiostat (VMP2, Bio-Logic) was used to perform the electrochemical measurements. All of the experiments were performed at room temperature (23 °C).

The film thickness was controlled by the deposition time, after proper calibration of the PECVD reactor [14], using optical measurements for determining refractive index and thickness of the deposited layer. Knowing the film thickness, the density of the material must be known to determine the mass of active material. A precise measurement of this density is not an easy task. Very few data are available in the literature. Solomon et al. [13] reported that the $x = 0.1$ compound density was 2 g cm^{-3}, compared to 2.25 g cm^{-3} for pure a-SiH. Williamson et al. studied materials very similar to ours [16]. They reported densities decreasing almost linearly from 2.26 for pure a-Si:H to 1.38 for a carbon content $x = 0.3$. Assuming this linear relationship, we estimated the following values for the different carbon contents used in this study: for $x = 0.1$, $d = 1.93$; for $x = 0.15$, $d = 1.79$; for $x = 0.20$, $d = 1.65$; for $x = 0.25$, $d = 1.51$ and for $x = 0.33$, $d = 1.29$.

After cycling, the cells were opened in the glove box, and the layers were rinsed successively in propylene carbonate and in a mixture of ethylene carbonate and dimethyl carbonate. They were dried under vacuum before post-mortem observation.

For infrared absorption measurements, $Si_{1-x}(CH_3)_x$:H layers were deposited on a crystalline silicon substrate (double-side polished parallel plate, 500 μm thickness, cut from a low-doped float-zone silicon wafer). The infrared transmission of the layers was measured using a non-polarized IR beam and at 45° incidence angle. This geometry allows to avoid the oscillations due to multiple reflections within the parallel-plate substrate, often observed when normal incidence is used. Layers with 0.1, 0.2, 0.3 and 0.37

carbon contents were prepared. A deposit was also prepared in the high-power regime (500 mW cm^{-2}) for comparison. The CH_4–SiH_4 proportion was the same as that used for the $x = 0.2$ Si–C compound prepared at low power.

4. Results and discussion

4.1. Infrared spectroscopy

Infrared vibrational spectroscopy is a sensitive tool for probing the local atomic environment, especially in the presence of light atoms such as hydrogen. Here, it may be expected that carbon is incorporated into the material in a variety of manners : at low x, carbon atoms are expected to appear isolated, coordinated either with a single silicon atom (Si–CH_3 groups) or with several silicon atoms (e.g., Si–CH_2–Si bridges). At higher carbon concentrations, carbon atoms bonded together may be present too, e.g., Si–CH_2–CH_3 groups, Si–CH_2–CH_2–Si bridges, or even unsaturated forms such as Si–CH=CH_2 and Si–CH=CH–Si bridges. Infrared spectroscopy can be used to discriminate between these different forms.

Infrared spectra recorded for our a Si–C layers are shown in Fig. 1. Carbon content is indicated for each spectrum. The spectrum at the bottom of each figure corresponds to the sample elaborated in the high-power plasma regime. The raw absorbance, recorded in the above stated conditions, was scaled to a layer of 1 μm thickness. In the following, we will successively discuss the C–H stretching region, the Si–H stretching region, the Si–C stretching region and the CH deformation region.

The change in shape of the spectrum with increasing x in the C–H stretching region (2800–3100 cm^{-1}) gives direct evidence for a change in the carbon atom hybridization state and in the nature of the CH groups. For a carbon atom in the sp3 hybridization state, two bands are expected for the CH_3 groups, the symmetric mode $\nu_S CH_3$ around 2885 cm^{-1} and the antisymmetric mode $\nu_{AS} CH_3$ around 2950 cm^{-1}. For the CH_2 groups, the corresponding bands are expected around 2860 and 2920 cm^{-1}. The exact positions of these bands slightly depend on the studied material and they partially overlap. Here, the two most prominent bands in the νCH spectra for $x = 0.1$ and 0.2 can clearly be identified with methyl stretching bands, indicating the dominant incorporation of carbon in the form of methyl groups. For larger x and for the high-power sample, the intensities of these two bands appear to decrease and a wide massif from 2850 to 2950 cm^{-1} grows up, which can be understood as the appearance of CH_2 groups. Furthermore, the stretching mode of unsaturated CH's (carbon atoms in the sp2 hybridization state), expected to appear between 3000 and 3100 cm^{-1}, can plausibly account for the growth of a wide absorption tail above 3000 cm^{-1}. Finally, note that the weak shoulder around 2800 cm^{-1}, mostly discernible at low x, can be identified with an overtone of a methyl deformation mode ($2\delta_{AS}CH_3$, enhanced by Fermi resonance), whereas the overtones of the CH_2 deformation modes are hidden below the νCH massif.

The Si–H stretching spectrum is dominated by a band centered around 2080 cm^{-1}. Attempts to fitting this spectrum indicate the presence of a weaker contribution, located around 2000 cm^{-1} for $x = 0.1$, and between 2100 and 2200 cm^{-1} for higher x. Note that the νSiH band in carbon-free amorphous hydrogenated silicon is located around 2000 cm^{-1}. The high-energy shift of the main band from 2000 to 2080 cm^{-1}, observed from $x = 0$ to $x = 0.1$, already reported in the literature [17], suggests a change from a bulk SiH to a surface SiH. It has been attributed to the appearance of nanovoids surrounding methyl groups, the hydrogen being preferentially incorporated at the surface of these nanovoids [16]. Our data are consistent with this interpretation. At higher x, we think that the appearance of a new contribution between 2100 and 2200 cm^{-1} may be attributed to the presence of one or several Si–C backbonds on the silicon bearing the hydrogen atom, a known effect of the presence of less electropositive substituents on silicon [18].

The Si–C stretching vibrations are expected to appear as a single band around 770 cm^{-1} for methyl groups [Si–(CH_3)], whereas two bands are expected for methylene bridges [Si–(CH_2)–Si] [19,20]. Here, the presence of a narrow band near 770 cm^{-1} for $x = 0.1$ and 0.2 stands as further evidence for the incorporation of carbon as methyl groups, whereas its broadening and the growth of a second band around 1100 cm^{-1} for larger x confirm the appearance of methylene bridges at high x.

Finally, the CH deformation spectra in the 1200–1500 cm^{-1} range appear even more prone to an unambiguous analysis, since the relevant bands do not overlap. In this range, the characteristic modes of the Si–CH_3 group are the symmetric "umbrella" mode

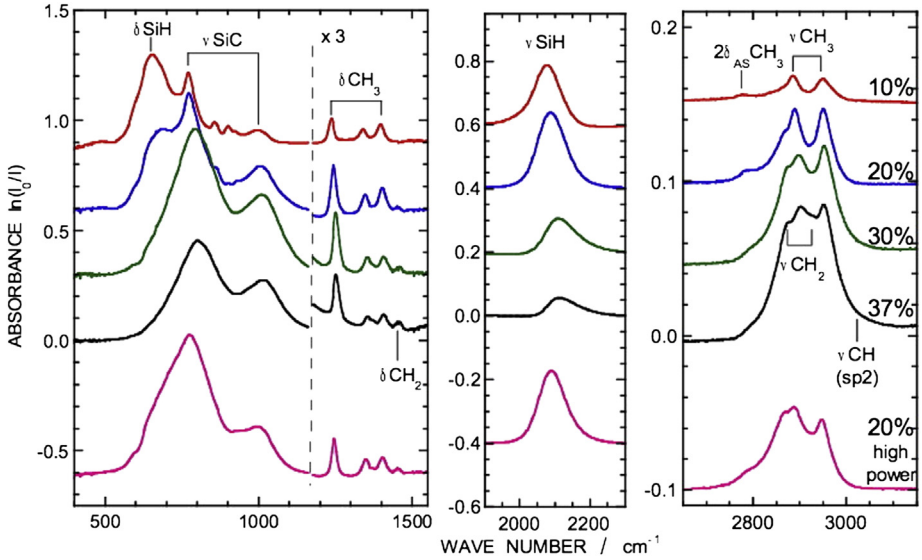

Fig. 1. Infrared spectra of a-$Si_{1-x}(CH_3)_x$:H layers obtained by PECVD in the low power (top) and high power (bottom) regimes. The spectra were obtained from transmittance measurements at 45° incidence angle of a layer deposited on a silicon substrate, and were scaled to a layer of 1 μm thickness. The value of x is indicated on each curve.

$\delta_S CH_3$, centered in the 1235–1250 cm^{-1} range, and the antisymmetric mode $\delta_{AS}CH_3$ around 1400 cm^{-1}. In contrast, a CH_2 group exhibits a single "scissor mode" around 1450 cm^{-1}, its wagging and rocking modes appearing below 1200 cm^{-1}. An examination of the spectra of Fig. 1 indicates that no measurable contribution from CH_2 groups is observed for $x = 0.1$, and an increasing contribution appears for $x = 0.2$ and above. However, an extra peak is observed between 1340 and 1360 cm^{-1}. This latter mode is often ascribed to Si–CH_2–Si bridges (see e.g., Ref. [21]). This assignment appears unlikely in the present case, since the amplitude of the peak is clearly correlated with the unambiguous (Si–)CH_3 contributions, and clearly not correlated with the (Si–)CH_2 ones. We rather suggest that this feature arises from a splitting of the doubly-degenerate $\delta_{AS}CH_3$ mode induced by an asymmetric environment of the methyl in the nanovoid surrounding it.

All in all, the infrared data confirm the dominant incorporation of carbon as methyl groups located inside hydrogen-coated nanovoids up to $x = 0.2$ and the appearance of CH_2 bridges and sp2 carbon at higher x. For the sample prepared with a high-power plasma, the spectra evidence a higher CH_2 content, compared to the low power regime.

4.2. Electrochemical properties

Fig. 2 compares the first cycles of 150 nm thick cells with $x = 0$ and $x = 0.1$. The current density is 6 μA cm^{-2}. We observe very similar curves, although with a slightly larger irreversible capacity for methylated Si than for pure a-Si:H. Variations of volumetric and gravimetric reversible capacities with carbon content are shown in Fig. 3a and b, respectively. Values shown for $0 \leq x \leq 0.2$ were obtained at charge/discharge rates of approximately C/10. The capacity was shown not to depend on layer thickness, within experimental errors: hence the values presented in Fig. 3 were averaged over series of layers with different thicknesses. For $x = 0.25$ and $x = 0.33$, we obtained very scattered results. Hence, in this figure we only include the maximum values obtained for these carbon contents, for comparison. The volumetric reversible capacity (Fig. 3a) is shown to decrease with increasing carbon content. The gravimetric reversible capacity (Fig. 3b) is almost constant up to $x = 0.15$, then it decreases. In particular, for the highest carbon contents (larger than 0.2), the capacity is much reduced, compared to pure Si. For this reason and because of the different nature of the material with $x > 0.2$ (higher content of CH_2 groups [13]), we did not investigate in detail the cycling behavior for the material with carbon content larger than 0.2.

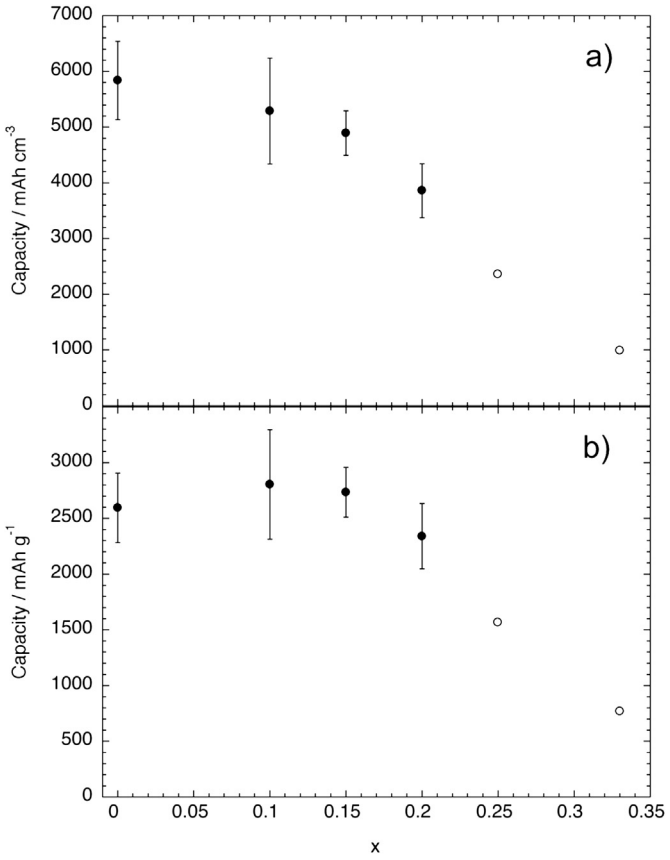

Fig. 3. a) Average volumetric reversible capacity (first cycle) of a-$Si_{1-x}(CH_3)_x$:H as a function of x. b) Average gravimetric reversible capacity as a function of x (same data as above).

Fig. 4 shows the variation of the reversible capacity of an a-$Si_{1-x}(CH_3)_x$:H layer with $x = 0.2$ as a function of the current density. A cell was cycled, starting at a current density of 2.9 μA cm^{-2}. Then the current density was gradually increased to 11.5 μA cm^{-2}, 23 μA cm^{-2}, and finally to 46 μA cm^{-2}, corresponding to a charge/

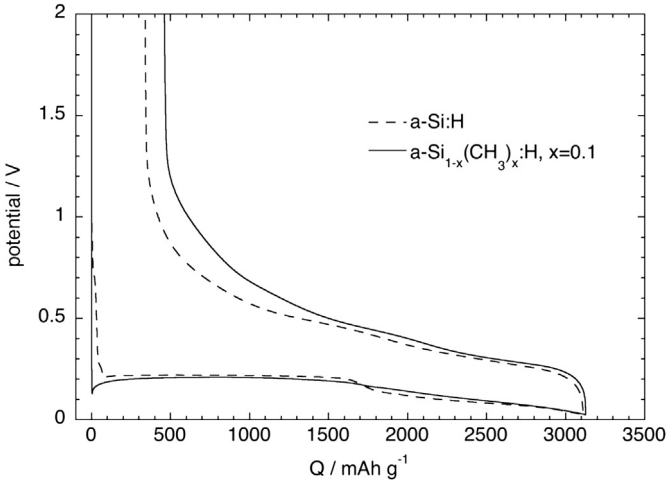

Fig. 2. First charge–discharge cycle of 150-nm thick electrodes: a-Si:H (dashed line); a-$Si_{1-x}(CH_3)_x$:H ($x = 0.1$, solid line). The current density is 6 μA cm^{-2}.

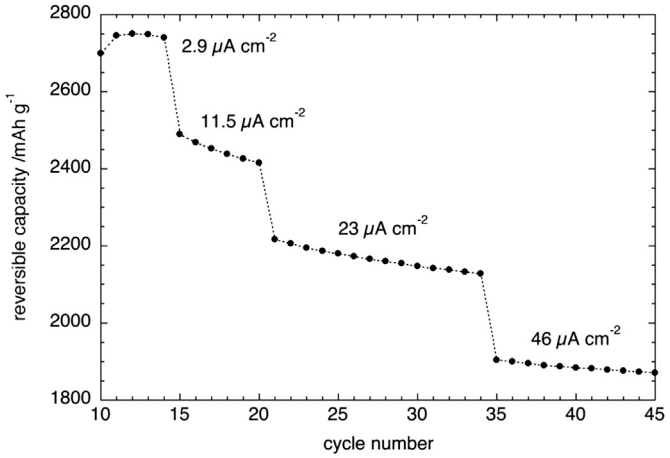

Fig. 4. Evolution of the reversible capacity of an a-$Si_{1-x}(CH_3)_x$:H layer, with $x = 0.2$, as a function of the cycle number: the current density is increased from 2.9 μA cm^{-2}–46 μA cm^{-2}. This last value corresponds approximately to a C/0.5 charge/discharge rate.

discharge rate of approximately C/0.5. As shown in Fig. 4, the capacity decreases with increasing the charge/discharge rate. This decrease is similar for pure a-Si:H and for a-$Si_{1-x}(CH_3)_x$:H.

As mentioned above, the first-cycle irreversible to reversible capacity ratio increases with increasing carbon content. As shown in Fig. 5, it decreases with increasing layer thickness. However, it tends to a non null value for the thickest layers: this was observed up to 600 nm. This indicates that the irreversible capacity has a double origin, one related to the surface of the layer (SEI formation), and one related to the bulk (trapping of lithium in the silicon network) [3].

Methylated Si layers display an enhanced cyclability compared to pure a-Si:H. Fig. 6a shows the capacity fading of two 70 nm layers, one with pure a-Si:H (closed circles), the other one with 10% carbon content ($x = 0.1$, open circles): the $x = 0.1$ layer is shown to sustain more than 250 cycles before loosing half of its initial capacity. Notice that at this stage, the capacity remains almost three times that of carbon electrodes. A similar trend is observed for other thicknesses. Another example is shown in Fig. 6b, for two 150 nm layers. As shown in the inset of Fig. 6a, the cyclability increases with increasing carbon content. For all carbon contents it decreases with increasing layer thickness. 60-nm thick electrodes with a carbon content $x = 0.2$ display a reversible capacity of nearly 2500 mA h g^{-1} and can sustain more than 300 cycles before loosing half of their initial capacity. With the same material, 300-nm thick electrodes can sustain 135 cycles before loosing half of their initial capacity.

The evolution of the coulombic efficiency for the $x = 0.1$ material is also shown in Fig. 6 for the 70 nm (Fig. 6a) and the 150 nm (Fig. 6b) thick layers. The coulombic efficiency first rapidly increases from an initial value of 0.91. After ten cycles it stabilizes to a value close to 0.97 in the 70 nm thick layer, 0.95 in the 150 nm thick layer. Similar behaviors were observed for all of the a-$Si_{1-x}(CH_3)_x$:H layers. This is in agreement with results reported by Kulova et al. [10] for pure a-Si:H layers obtained in similar conditions. The fading of the capacity is too slow for directly accounting for this value. The limited coulombic efficiency is therefore associated with irreversible reactions taking place at the electrode interphase which consume a small part of the charging current. This point has been discussed in detail in Ref. [3].

As in the case of pure amorphous silicon [22–25], crack pattern formation may be observed in thick layers, giving rise to separated flakes. Post-mortem observation was performed by optical microscopy (Fig. 7) and by non-contact Atomic Force Microscopy (nc-AFM, Fig. 8). In Figs. 7a and 8 are shown respectively an optical microscopy image and an AFM image of an a-$Si_{1-x}(CH_3)_x$:H, $x = 0.2$ layer, of thickness 300 nm, after 60 charge/discharge cycles: these images were obtained after complete delithiation of the sample. In Fig. 7a, one observes that the flakes formed by the cracking have a size ranging from a few μm to about 20 μm. Fig. 8 shows that these flakes curl up at their edge, indicating that their edge tends to become disconnected from the substrate. A similar observation was obtained by Beaulieu et al. [22].

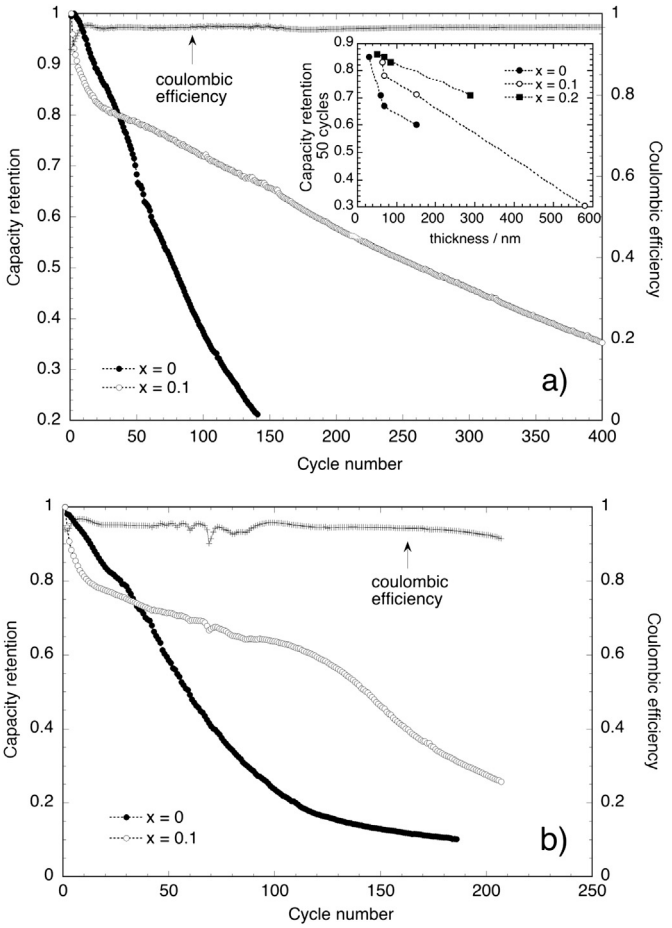

Fig. 6. a) Capacity decrease with cycle number for two 70 nm layers: $x = 0$ (closed circles), $x = 0.1$ (open circles). Coulombic efficiency (crosses) is also shown for the $x = 0.1$ layer. The current density is 16 μA cm^{-2}. Inset: variation of the capacity retention after 50 cycles as a function of the layer thickness for $x = 0$, $x = 0.1$ and $x = 0.2$. b) Capacity decrease and variation of Coulombic efficiency for the $x = 0.1$ material with cycle number for two 150 nm layers: same symbols as above. The current density is 22.5 μA cm^{-2}.

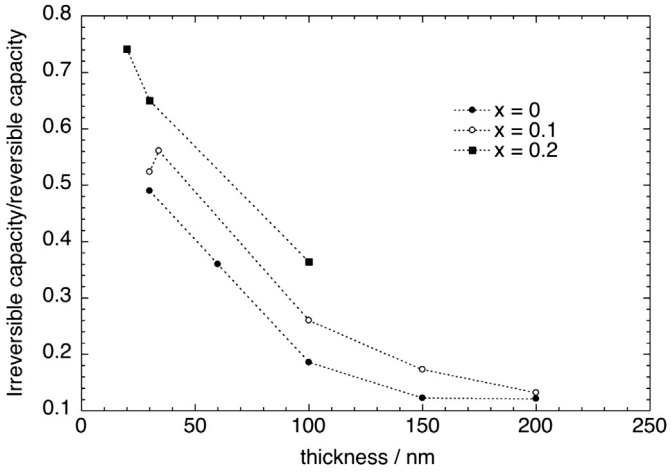

Fig. 5. Irreversible capacity to reversible capacity ratio as a function of layer thickness for $x = 0$, $x = 0.1$ and $x = 0.2$.

Cracks appear at the very first cycle. However, only a disconnected network of cracks is then observed (Fig. 7b). For the highest layer thickness (600 nm), the layers crack into small grains. The layer then appears to be partially disconnected from the substrate.

The minimum thickness above which cracks are observed appears to depend on carbon content. Although a systematic investigation was not performed as a function of layer thickness, we found that for three carbon contents ($x = 0$, $x = 0.1$ and $x = 0.2$) and three layer thicknesses (70 nm, 150 nm, 300 nm), the results were as follows. For $x = 0$, cracks were observed in all cases. For $x = 0.1$, cracks were not observed in the 70 nm layers, but they were observed in thicker layers. For $x = 0.2$, cracks were only observed in the thick layers (300 nm). This property could straightforwardly be related to the material atomic structure. Methyl groups are

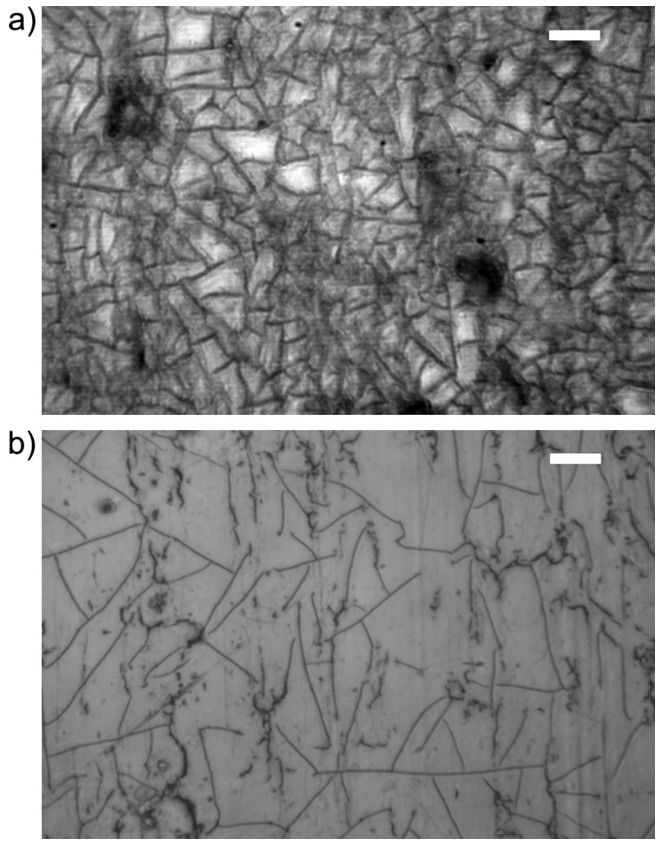

Fig. 7. Post-mortem optical microscopy image of a-$Si_{1-x}(CH_3)_x$:H, $x = 0.2$ layer. The layer is 300 nm thick. The white bar is 10 μm long. a) After 60 cycles (current density 10 μA cm^{-2}) b) after 3 cycles (current density 15 μA cm^{-2}).

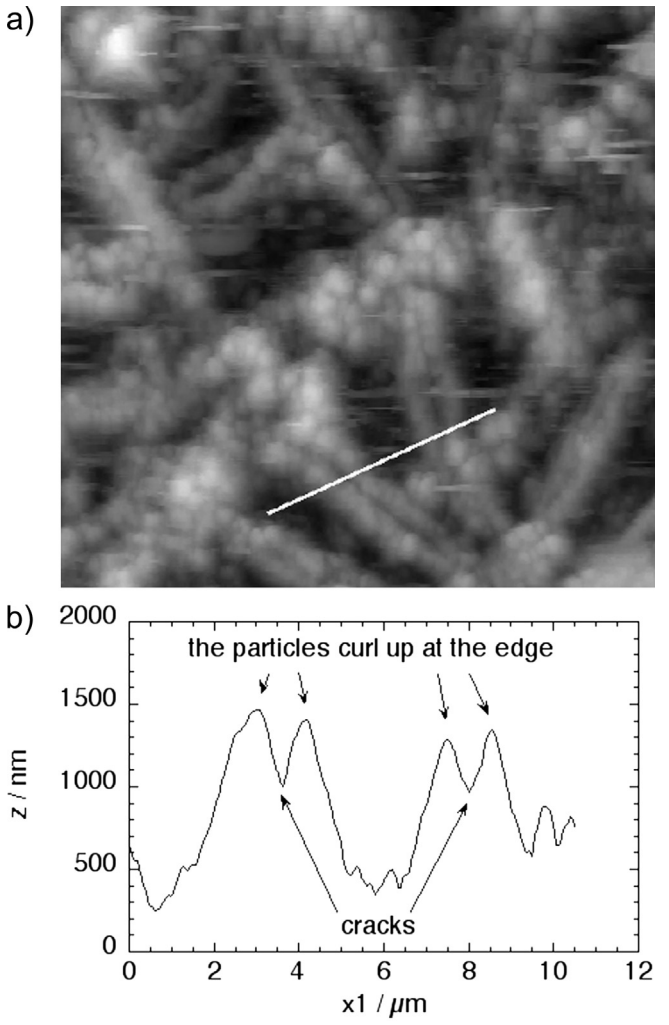

Fig. 8. nc-AFM topography observation of the same sample as in Fig. 7a: a) AFM image (size 25 × 25 μm^2) b) cross section along the white line shown in Fig. 8a: the flakes are seen to curl up at their edge.

monovalent species and can only be linked to one silicon atom, thus creating dead ends in the silicon network and reducing the average number of Si–Si bonds in the three-dimensional silicon network of a-$Si_{1-x}(CH_3)_x$:H. This reduction of the average coordination number of silicon atoms, as well as the presence of nanovoids surrounding methyl groups, should make the material softer than a-Si:H or crystalline Si, and less sensitive to volume variations induced by the intercalation/de-intercalation of lithium, accounting for the better cyclability experimentally obtained. Indeed, in hybrid materials, addition of organic substituents and specifically CH_3, was shown to notably change mechanical properties of materials and make them softer as compared to the corresponding purely inorganic phase [26]. The presence of microporosity may also be expected to similarly affect these properties: Roberts and Garboczi [27] calculated that a porosity of 10% would decrease the Young modulus of a material by about 25% whatever the geometry is. However, a more detailed study is required for making such arguments quantitative and precisely understanding crack pattern formation as a function of carbon content and layer thickness.

One may also wonder whether the enhanced cyclability observed for our material could be due to its sole porosity. Indeed porosity was shown to improve Si cyclability (see for example Ref. [28]). However this is true for a large porosity, leaving room enough for the material expansion due to lithium insertion: we are very far from these conditions in our case, where porosity is very low. For example for a carbon content of 10%, the density values of our material (1.93–2 g cm^{-3}) point to a porosity ranging between 5 and 9%.

The rapid decrease of the capacity of the material for $x > 0.2$ might be related to the presence of CH_2 groups, because Si–CH_2–Si units are expected to reticulate the Si network, hence reducing the number of available space for lithium intercalation. It probably also makes the amorphous material more rigid.

5. Conclusion

PECVD from SiH_4 and CH_4 enables one to produce easily obtainable, amorphous methylated silicon a-$Si_{1-x}(CH_3)_x$:H with x in the range $0 \leq x \leq 0.33$. Up to $x = 0.2$, the carbon is mostly inserted as methyl groups CH_3. Thin layers of this material were shown to constitute anodes for Li-ion batteries with increased cyclability, with almost no loss of gravimetric capacity. Compared with pure a-Si:H, a twofold improvement was obtained:

- longer lifetime
- capability of working with thicker electrodes

The observed improvement is attributed to mechanical softening of amorphous Si by the incorporation of CH_3 groups.

Note that, in this paper, the performances of this material were compared to those of amorphous silicon prepared and operated in a comparable manner: extra advantages may be expected if using it in divided form, or in replacement of pure silicon in the different

recent implementations which were proposed to improve silicon cyclability [3].

Acknowledgments

The authors wish to thank Dominique Clément for the mechanical realization of the different electrochemical cells used in this work.

References

[1] M.N. Obrovac, L. Christensen, D.B. Le, J.R. Dahn, J. Electrochem. Soc. 154 (2007) A849–A855.
[2] U. Kasavajjula, C. Wang, A.J. Appleby, J. Power Sources 163 (2007) 1003–1039.
[3] W.-J. Zhang, J. Power Sources 196 (2011) 13–24.
[4] K.T. Lee, J. Cho, Nano Today 6 (2011) 28–41.
[5] V.A. Sethuraman, K. Kowolik, V. Srinivasan, J. Power Sources 196 (2011) 393–398.
[6] M. Uehara, J. Suzuki, K. Tamura, K. Sekine, T. Takamura, J. Power Sources 146 (2005) 441–444.
[7] Z. Du, S. Zhang, T. Jiang, R. Lin, J. Zhao, Electrochim. Acta 74 (2012) 222–226.
[8] S.K. Soni, B.W. Sheldon, X. Xiao, A. Tokranov, Scr. Mater. 64 (2011) 307–310.
[9] R.A. Street, Hydrogenated Amorphous Silicon, Cambridge University Press, 1991.
[10] T.L. Kulova, A.M. Skundin, Yu.V. Pleskov, E.I. Terukov, O.I. Kon'kov, J. Electroanal. Chem. 600 (2007) 217–225.
[11] J. Saint, M. Morcrette, D. Larcher, L. Laffont, S. Beattie, J.-P. Pérès, D. Talaga, M. Couzi, J.-M. Tarascon, Adv. Funct. Mater. 17 (2007) 1765–1774.
[12] A.L. Lipson, S. Chattopadhyay, H.J. Karmel, T.T. Fister, J.D. Emery, V.P. Dravid, M.M. Thackeray, P.A. Fenter, M.J. Bedzyk, M.C. Hersam, J. Phys. Chem. C 116 (2012) 20949–20957.
[13] I. Solomon, M.P. Schmidt, H. Tran-Quoc, Phys. Rev. B 38 (1988) 9895–9901.
[14] I. Solomon, M.P. Schmidt, C. Sénémaud, M.D. Khodja, Phys. Rev. B 38 (1988) 13263–13270.
[15] M.L. de Oliveira, S.S. Camargo, F.L. Freire, J. Appl. Phys. 71 (1992) 1531–1533.
[16] D.L. Williamson, A.H. Mahan, B.P. Nelson, R.S. Crandall, Appl. Phys. Lett. 55 (1989) 783–785.
[17] A.H. Mahan, P. Raboisson, D.L. Williamson, R. Tsu, Solar Cells 21 (1987) 117–126.
[18] D.V. Tsu, G. Lucovsky, B.N. Davidson, Phys. Rev. B 40 (1989) 1795–1805.
[19] D. Lin-Vien, N.B. Colthup, W.G. Fateley, J.G. Grasselli, The Handbook of Infrared and Raman Frequencies of Organic Molecules, Academic Press, San Diego, CA, 1991, pp. 251–261.
[20] F. Ozanam, C. Vieillard, M. Warntjes, T. Dubois, M. Pauly, J.-N. Chazalviel, Can. J. Chem. Eng. 76 (1998) 1020–1026.
[21] A. Grill, D.A. Neumayer, J. Appl. Phys. 94 (2003) 6697–6707.
[22] L.Y. Beaulieu, K.W. Eberman, R.L. Turner, L.J. Krause, J.R. Dahn, Electrochem. Solid State Lett. 4 (2001) A137–A140.
[23] Y. He, X. Yu, G. Li, R. Wang, H. Li, Y. Wang, H. Gao, X. Huang, J. Power Sources 216 (2012) 131–138.
[24] J.P. Maranchi, A.F. Hepp, A.G. Evans, N.T. Nuhfer, P.N. Kumta, J. Electrochem. Soc. 153 (2006) A1246–A1253.
[25] J. Li, A.K. Dozier, Y. Li, F. Yang, Y.-T. Cheng, J. Electrochem. Soc. 158 (2011) A689–A694.
[26] A.J. Atanacio, B.A. Latella, C.J. Barbé, M.V. Swain, Surf. Coat. Technol. 192 (2005) 354–364.
[27] A.P. Roberts, E.J. Garboczi, Proc. R. Soc. Lond. A 458 (2002) 1033–1054.
[28] H. Kim, B. Han, J. Choo, J. Cho, Angew. Chem. Int. Ed. 47 (2008) 10151–10154.